Progress In Electromagnetics Research C, Vol. 125, 133–146, 2022

A Taguchi-Preconditioned GA Method for the Design Optimization of a PM Vernier Motor

Gaojia Zhu[1], Shijie Liu[1], Longnv Li[1, *], Yishuang Zhao[1], Shengyang Hu[1], and Yiran Yun[2]

Abstract—This paper presents an efficient Taguchi-preconditioned genetic algorithm (TPGA) strategy for the design optimization of a 630-kW permanent magnet vernier motor (PMVM). In the TPGA, firstly, the Taguchi method is combined with comparative finite element analyses (FEA) to judge the influence factors of six typical structural parameters on the torque output. Secondly, four influential parameters are taken from the six typical ones and decided as the variables in the global optimization processes coupling genetic algorithm (GA) and FEA. As two variables with small influence factors are set to constants in the computationally costly optimization processes, the calculation burden can thus be effectively reduced. Thirdly, with the four influential optimization variables, FEA-assisted GA is used to maximize the output torque of the PMVM. During the global optimization processes, a preliminarily optimized structural configuration obtained from the Taguchi analyses is used as the initial values of the variables. Finally, the working performances of the machine with the optimal parameters are obtained through FEM calculations. The optimization effectiveness is validated by comparing the output torque of the GA-optimized machine with that of the initial and the Taguchi-preliminary optimized ones.

1. INTRODUCTION

In modern civilized and industrial applications, low-speed and large-torque-density operations are usually demanded. To provide sufficient driving torques without enlarging the driving system sizes, mechanical gearboxes are often connected with driving motors to slow down the rotation speeds while magnifying the output torques [1, 2]. However, due to the inevitable mechanical frictions between the gears, the working reliability and the operation efficiencies of the systems using gearboxes are seriously limited [3, 4].

To realize the torque transformations without mechanical speed-regulating devices, magnetic gears based on the flux modulation theory have been utilized to supersede the mechanical gears in [5, 6]. Since vernier machines (VMs) can use the stator slots as iron segments and thus integrate the magnetic gears into the machine casings, they have attracted extensive research attentions in the direct-drive and large-torque applications [7, 8].

1.1. State-of-the-Art

In order to maximize the output torque of VMs, researches have been done in designing and optimizing the machine configurations. In [9], Toba and Lipo proposed the element domain (ED) model for a permanent magnet vernier motor (PMVM), and the generic design for maximizing the output torque was realized based on the ED methodologies. Zhao et al. [10] presented the quantitative analyses and design guidelines for dual-permanent-magnet vernier machines (DPMVMs), and the results were validated

Received 19 July 2022, Accepted 10 October 2022, Scheduled 13 October 2022
* Corresponding author: Longnv Li (lilongnv@tiangong.edu.cn).
[1] School of Electrical Engineering, Tiangong University, Tianjin 300387, China. [2] State Grid Tianjin Ninghe Electric Power Supply Company, Tianjin, China.

through numerical and experimental researches. In [11], Ma et al. proposed a surrogate-assisted design optimization scheme to realize the efficient multi-objective optimization of a surface-mounted PMVM. In the multi-criteria optimization processes, the surrogate-assisted techniques were used to improve the computational efficiency. Among the modern optimization methods, genetic algorithm (GA) is most commonly used in optimizing VMs for its superior advantage in global searching [12, 13]. In [14], Lin et al. proposed the numerical presentations for the design configurations of a DPMVM and optimized the numerical sets through GA. Wang et al. [15] investigated the influences of the structural parameters of an axial-flux PMVM on the output torque and axial electromagnetic force. A Kriging prediction method was utilized to model the influences, and GA was combined with the prediction model to search for an optimized result.

For the design optimization of VMs, since the relations between the electromagnetic fields and the machine parameters are highly nonlinear [9], the output performances of the machines can hardly be modeled by analytical models. Therefore, the most usual way in optimizing them is to combine the optimization algorithms with numerical calculations, making the whole processes computationally costly [14, 15]. In addition, due to the complex structures of VMs, a large number of variables need to be selected during optimization processes, which will further increase the complexities and the calculation burdens.

Through the design of experiment (DOE) methods, such as the Taguchi method [16], response surface methodology (RSM) [17] and Latin hypercube sampling strategy [18], the optimal combination of machine structural parameters can be obtained based on limited times of numerical calculations. Amongst the DOE methods, the Taguchi method is more commonly utilized in the designs of electrical machines for its preferable characteristics of reliability, conciseness, and robustness [19, 20]. In [21], Khan et al. combined manufacturing tolerances with assembly process variations in the optimal design of a surface-mounted PMSM based on Taguchi method. Xia et al. [22] employed the Taguchi method to optimize the PM cavity under different working conditions. In [23], Shi et al. novelly considered the fault-tolerate capability in the Taguchi-based design optimization of a five-phase PM hub motor. By using Taguchi method, the optimized design of a PMSM can be obtained efficiently. But as the designed values based on Taguchi method are received with only dozens or even fewer simulation results, they usually have quite an adequate potential to be further optimized.

1.2. Contributions

To overcome the aforementioned problems, in this paper, a Taguchi-preconditioned method is proposed to realize the efficient FEA-assisted GA optimization of a PMVM. The detailed contributions in this paper are as follows:

(1) Through variance proportion analyses based on Taguchi method, the approach in obtaining the influential factors of PMVM structural parameters on the output performances is proposed.
(2) Taking the most influential variables obtained by Taguchi analyses in the FEA-assisted GA optimizations, the calculation burden cost in the FEM simulations is effectually reduced.
(3) Combining the aforementioned contributions, the Taguchi-preconditioned genetic algorithm (TPGA) is proposed to realize the efficient and effective optimizations of PMVMs.

2. 2 PMVM AND INITIAL WORKING PERFORMANCES

2.1. Machine Structure and Initial Parameters

The PMVM studied in this paper is with an outer-rotor and inner-stator structure, as shown in Fig. 1. Silicon steel sheets with brand 35W470 are employed to make the stator and rotor cores. The stator core has 36 rectangular slots, which are also used as iron segments to modulate the air-gap flux. The basic parameters of the machine are tabulated in Table 1.

2.2. Initial Working Performance Analyses

The transient electromagnetic field of the machine is obtained by FEM calculations, and the flux line and flux density distributions are shown in Fig. 2, illustrating the flux modulation effect transforming

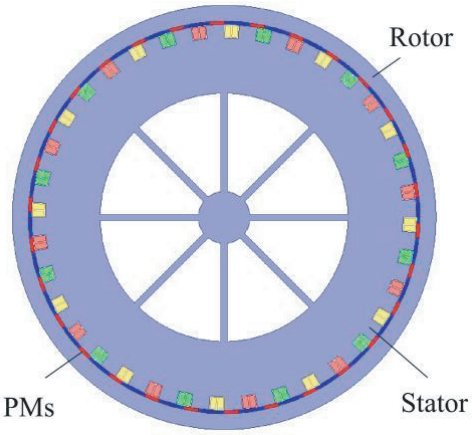

Figure 1. Machine structure.

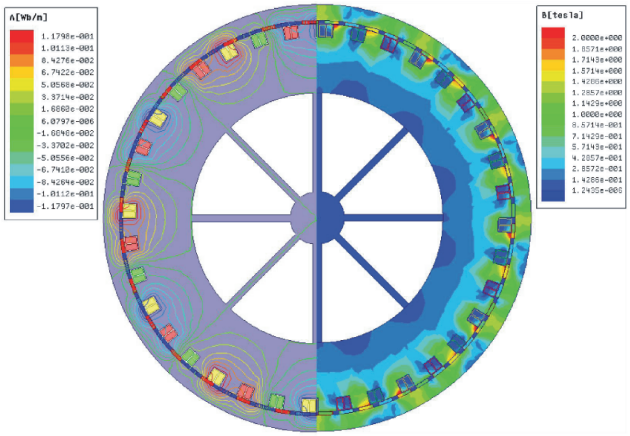

Figure 2. Flux lines and flux density distributions of the PMVM.

Table 1. Initial parameters of PMVM.

Quantity	Value
Axial length	750 mm
Outer diameter of rotor	2660 mm
Inner diameter of rotor	2460 mm
PM height	20 mm
Air-gap length	1 mm
Outer diameter of stator	2418 mm
Inner diameter of stator	779 mm
Slot width (in radians)	5.5°
Rotor pole pair number	30
Slot (iron segment) number	36
Stator pole pair number	6

the 30 paired magnetic fluxes in rotor to the 6 paired ones in stator. Fig. 3 shows the output torque of the machine versus time. The PMVM can provide an averaged torque (T_{ave}) of 283.93 kN·m, which means a high torque density at 68.12 kN·m/m^3. In addition, the torque ripple of the machine can be maintained below 1.32% (T_{rip} at 3.73 kN·m) under full load operations. The calculated working performances of the machine are tabulated in Table 2.

Table 2. Working performances of the PMVM.

Parameter	T_{ave}/kN·m	T_{rip}/kN·m	U_{ave}/kV
Value	283.93	3.73	11.4

3. DESIGN OPTIMIZATION BASED ON TPGA

3.1. Methodologies

Starting from the initial structural parameters of the VM, in this section, the TPGA is proposed and employed to realize the efficient optimization of the machine. The detailed optimization processes are

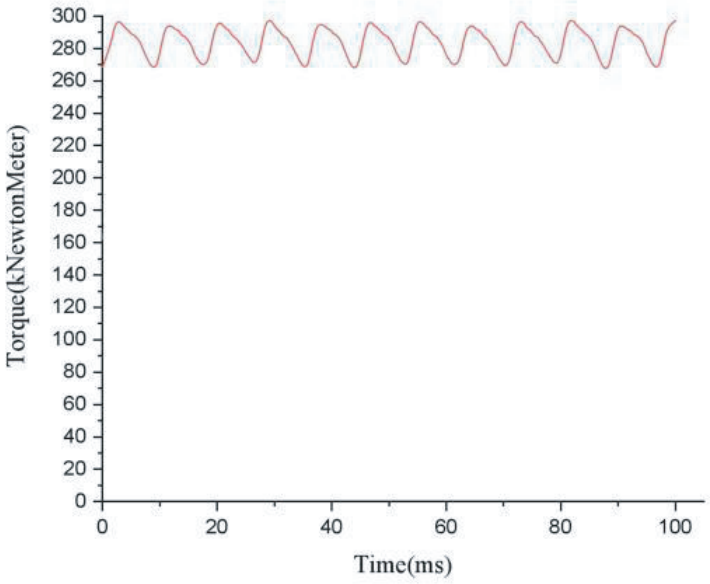

Figure 3. The output torque versus time (initial).

illustrated in Fig. 4, and the optimization steps are as follows:

(1) With the initial parameters and material properties inputted, six typical structural parameters (rotor yoke depth, d_{rotor}, stator yoke depth, d_{stator}, air-gap length, l_{gap}, stator tooth height, h_{st}, PM height, h_{PM}, and stator tooth width, w_{st}) that have relatively large impacts on machine electromagnetic characteristics are selected as the initial optimization variables in the Taguchi-based analyses.

(2) The $L5^6$ orthogonal table is established with related machine working performances calculated through FEM. Taguchi method is then employed to analyze the influence factor of each variable.

(3) The four most influential structural parameters are selected from the six typical ones and are used as the variables in GA-based optimization. In addition, the preliminary structural configuration obtained by Taguchi method is used as the initial value in the globalized optimization processes.

(4) The GA setup is established based on the aforementioned variables and initial values. The variation ranges are also decided based on Taguchi analyses.

(5) FEM calculations are combined with GA to globally optimize the machine structural parameters. The finally optimized structural configuration is exported for FEA.

3.2. Taguchi-Based Preconditioning Processes

3.2.1. Basic Conditions

For the Taguchi analyses, six typical structural parameters are selected as the optimization variables. Several constraints are set on the ranges of the variables:

(1) A smaller depth of the rotor yoke will lead to heavy saturation and significant reduction on the PMVM performance. When selecting the depth of the rotor yoke, it is necessary to ensure that the averaged magnetic flux density in the rotor is less than 1.8 T.

(2) When being deposited with a large air gap, the excitation current has to increase to fix with increasing magnetic resistances. However, to balance the manufacturing precision, the air gap length should also be not too small.

(3) The PM consumption is set to constant during optimization. Therefore, reducing the height of the PMs will make them wider. In order to avoid the overlapping of the adjacent PMs, the minimum height of the PMs is 14.6 mm.

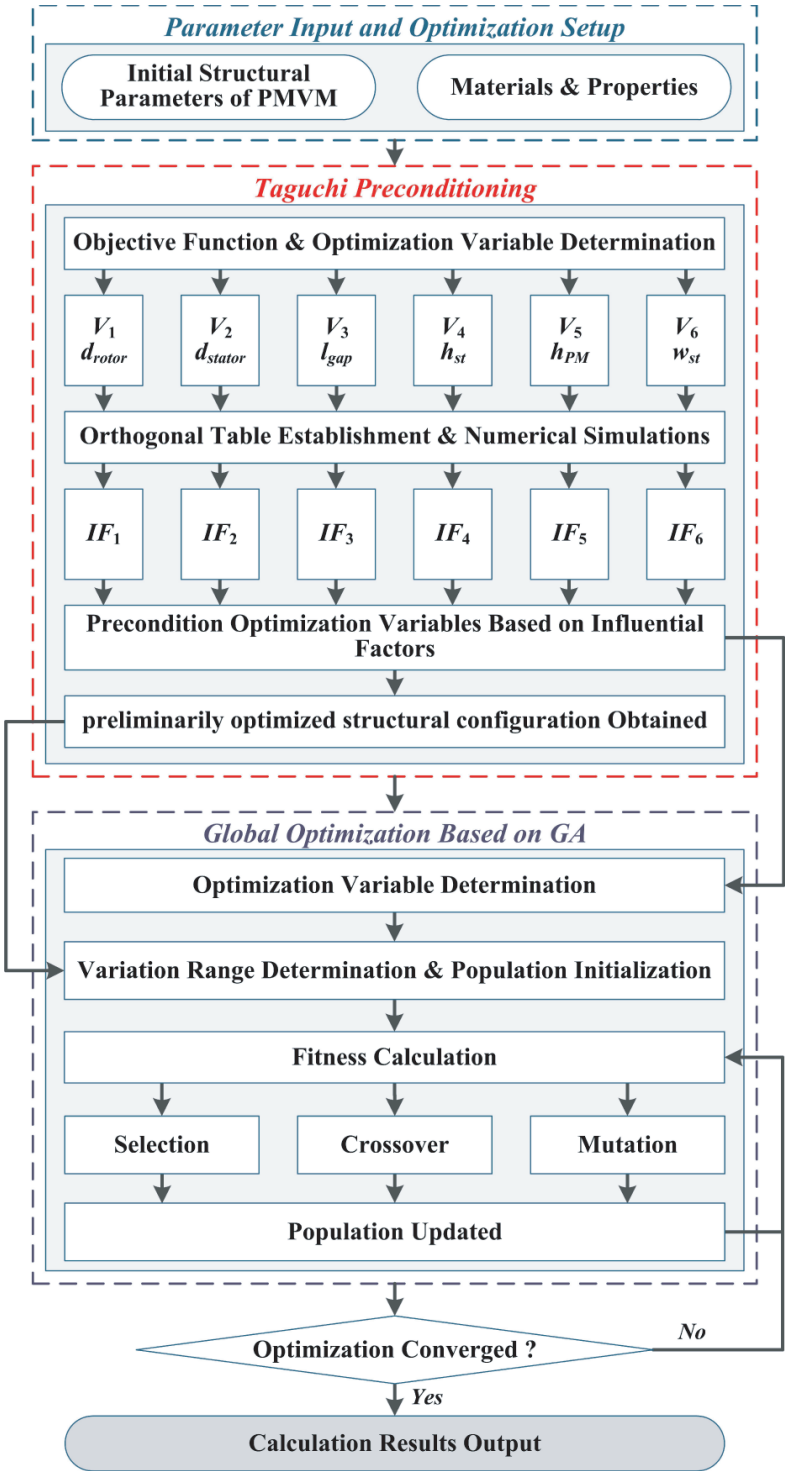

Figure 4. Optimization process flowchart.

(4) The width of the stator teeth has a significant influence on the electromagnetic performances of the motor. Since 36 stator teeth separate 360° space, the stator teeth width is constrained from 3° to 7° to leave spare space for stator windings.

3.2.2. Analyzing and Preconditioning Process

For the globalized robust design optimization of the PMVM through GA, due to the complex machine structure and large machine size, the selection of the optimization variables has become a hard task. Too many optimization variables will lead to slow convergence speed with large amounts of numerical calculations. A small variable number will in turn lead to an insufficient optimization effort. To balance those contradictions, Taguchi method is used to diminish the least influential variables by judging their influence factors and to obtain a fine initial value for the GA-based optimizations.

Figure 5 shows the schematic diagram of optimized variables. In order to implement this method, the optimal range and levels of the variables are presented in Table 3 and Table 4, respectively. As shown in the tables, six variables with five levels of each variable are selected. The related orthogonal table is set up as shown in Table 5. The averaged output torque (T_{ave}) and the value of torque ripple (T_{rip}) with according levels are calculated and also listed in the table.

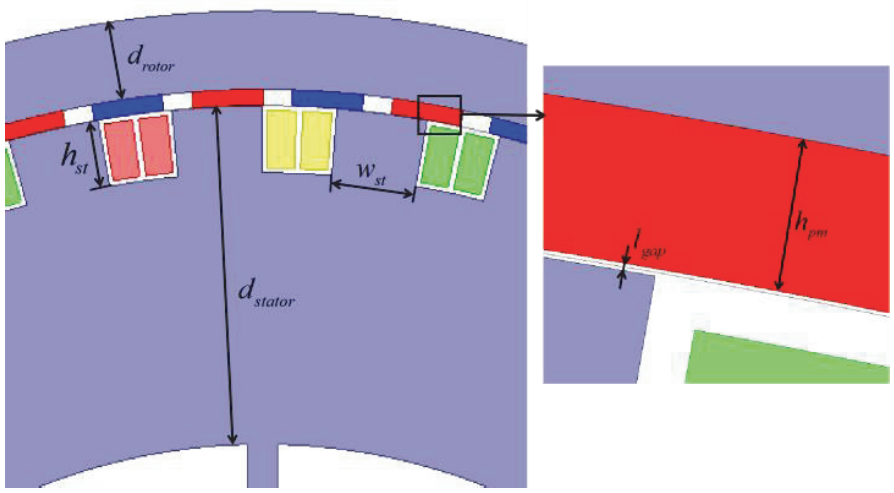

Figure 5. Schematic diagram of optimized variables.

Table 3. Optimal range of factors.

Variable	Description	Range
d_{rotor}/mm	Rotor yoke depth	$60 \sim 140$
d_{stator}/mm	Stator yoke depth	$325 \sim 405$
l_{gap}/mm	Air gap length	$0.9 \sim 1.3$
h_{st}/mm	Stator teeth height	$80 \sim 120$
h_{PM}/mm	PM height	$14.6 \sim 18.6$
w_{st}/deg	Stator teeth width (in radians)	$3° \sim 7°$

In order to analyze the influential factors on the optimization variables, the averaged T_{ave} and T_{rip} with different levels of each variable are analyzed and listed in Table 5. For example, the averaged value of the output torque with a 1-level d_{rotor} can be obtained by:

$$T_{ave}(\delta_1) = \frac{T_{ave}(1) + T_{ave}(2) + T_{ave}(3) + T_{ave}(4) + T_{ave}(5)}{5} \tag{1}$$

where $T_{ave}(1)$, $T_{ave}(2)$, $T_{ave}(3)$, $T_{ave}(4)$, and $T_{ave}(5)$ are the output torque average in experiments 1, 2, 3, 4, and 5, respectively.

The proportion of the influence factors of each variable on T_{ave} and T_{rip} can be obtained by variance analyses. In the variance analyses, the overall average value (SS) of each objective function should be

Table 4. Factor level value.

Level Variable	1	2	3	4	5
d_{rotor}/mm	60	80	100	120	140
d_{stator}/mm	325	345	365	385	405
l_{gap}/mm	0.9	1	1.1	1.2	1.3
h_{st}/mm	80	90	100	110	120
h_{PM}/mm	14.6	15.6	16.6	17.6	18.6
w_{st}/deg	3°	4°	5°	6°	7°

Table 5. $L5^6$ orthogonal table and related working performances calculated.

No.	Combinations of variable levels						T_{ave}/kN·m	T_{rip}/kN·m
	d_{rotor}/mm	d_{stator}/mm	l_{gap}/mm	h_{st}/mm	h_{PM}/mm	w_{st}/deg		
1	1	1	1	1	1	1	168.44	10.84
2	1	2	2	2	2	2	255.64	8.02
3	1	3	3	3	3	3	276.75	4.33
4	1	4	4	4	4	4	253.97	6.13
5	1	5	5	5	5	5	209.54	4.29
6	2	1	2	3	4	5	246.24	5.51
7	2	2	3	4	5	1	213.61	8.42
8	2	3	4	5	1	2	236.03	14.15
9	2	4	5	1	2	3	294.48	3.58
10	2	5	1	2	3	4	294.60	7.43
11	3	1	3	5	2	4	300.61	8.49
12	3	2	4	1	3	5	263.41	5.96
13	3	3	5	2	4	1	198.38	6.69
14	3	4	1	3	5	2	268.27	3.23
15	3	5	2	4	1	3	282.74	6.23
16	4	1	4	2	5	3	288.25	4.57
17	4	2	5	3	1	4	287.28	10.70
18	4	3	1	4	2	5	274.57	4.41
19	4	4	2	5	3	1	183.83	4.22
20	4	5	3	1	4	2	256.00	4.39
21	5	1	5	4	3	2	242.37	8.42
22	5	2	1	5	4	3	288.13	4.25
23	5	3	2	1	5	4	279.78	4.33
24	5	4	3	2	1	5	269.38	3.45
25	5	5	4	3	2	1	156.92	9.96

calculated first. Take T_{ave} as an example:

$$SS\left(T_{ave}\right) = \frac{1}{25}\sum_{1}^{25} T_{ave}(i) \tag{2}$$

where $T_{ave}(i)$ is the output torque in the ith combination in Table 6. The variance (SSF) is then

Table 6. The average value of torque under different levels of each optimization factor.

Variable	level	T_{ave}/kN·m	T_{rip}/kN·m
d_{rotor}/mm	1	232.87	6.72
	2	256.99	7.82
	3	262.68	6.12
	4	257.99	5.66
	5	247.32	6.08
d_{stator}/mm	1	249.18	7.57
	2	261.61	7.47
	3	253.10	6.78
	4	253.99	4.12
	5	239.96	6.46
l_{gap}/mm	1	258.80	6.07
	2	249.65	5.66
	3	263.27	5.82
	4	239.72	8.15
	5	246.41	6.74
h_{st}/mm	1	252.42	5.82
	2	261.25	6.03
	3	247.09	6.75
	4	253.45	6.72
	5	243.63	7.08
h_{PM}/mm	1	248.77	9.07
	2	256.44	6.45
	3	252.19	6.07
	4	248.54	5.39
	5	251.89	4.97
w_{st}/deg	1	184.24	8.03
	2	251.66	7.64
	3	286.07	4.59
	4	283.25	7.42
	5	252.63	4.72

obtained by:

$$SSF(T_{ave}) = \frac{1}{n}\sum_{i=1}^{n}\left(T_{ave}(i) - SS(T_{ave})\right)^2 \tag{3}$$

where n is the number of the levels. Similarly, the variance and influential factor of each variable are calculated. The calculation results are shown in Table 7.

As can be found from the results, variable w_{st} has the largest impact on the output torque, and level 3 shows the best result. Therefore, variable w_{st} is selected in the GA-based optimizations. On the contrary, the stator tooth height has a relatively small influence on the output torque, and it is not taken as an optimization variable in the later globalized optimizations. The rest variables affect the output torque more significantly than factor h_{pm}. Therefore, variables d_{rotor}, d_{stator}, l_{gap}, and w_{st} are further optimized to maximize the PMVM output torque.

Table 7. The variance and the influential factors of each optimization factor under different performance indexes.

Factors	T_{ave}/kN·m		T_{rip}/kN·m	
	Variance	Influential factor/%	Variance	Influential factor/%
d_{rotor}/mm	112.36	6.92	0.57	7.58
d_{stator}/mm	49.90	3.07	1.57	20.88
l_{gap}/mm	71.98	4.43	0.83	11.04
h_{st}/mm	36.21	2.23	0.23	3.06
h_{pm}/mm	8.24	0.51	2.06	27.39
w_{st}/deg	1345.6	82.84	2.26	30.05
total	1624.36	100	7.52	100

3.2.3. Initial Value and Ranges

Figure 6 shows the factor effects on torque and torque ripple. The initial value and variation range of each variable are decided based on the figures. For factors h_{st} and h_{PM} shown in Figs. 6(d) and (e), the initial values are set to 90 mm and 18.6 mm, respectively.

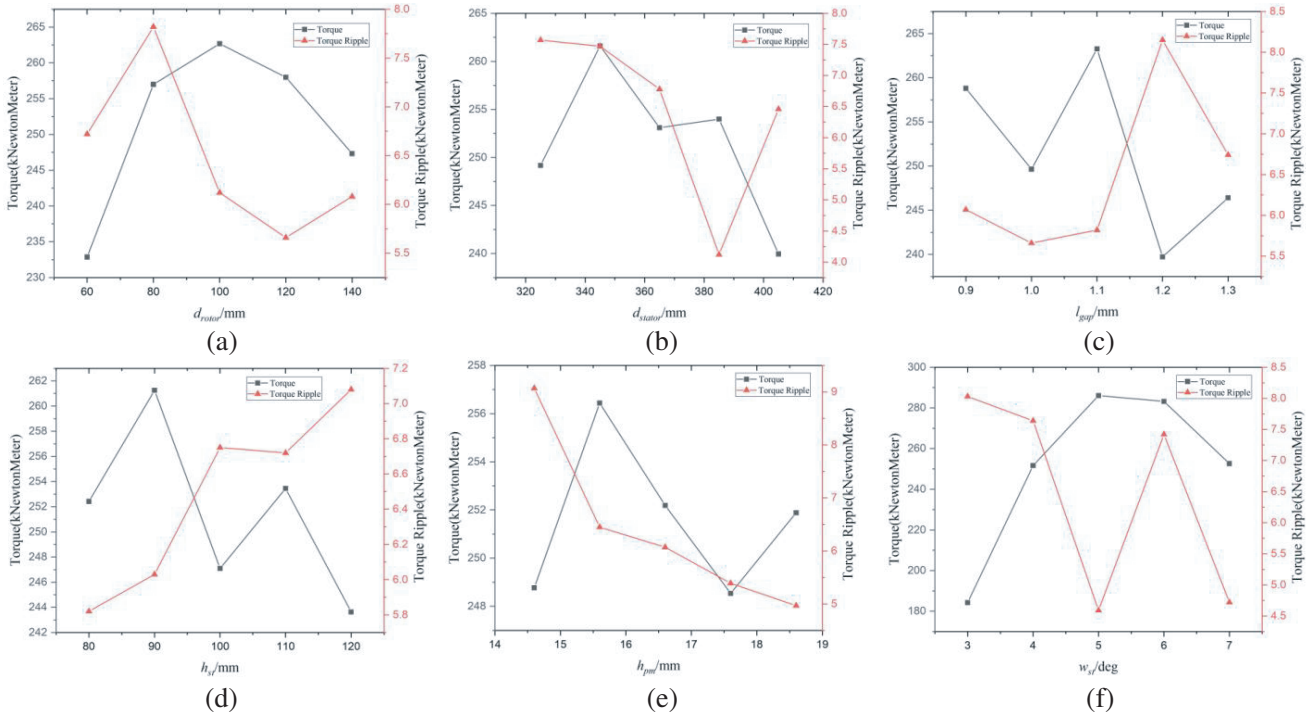

Figure 6. Factor effects on torque and torque ripple. (a) d_{rotor}. (b) d_{stator}. (c) l_{gap}. (d) h_{st}. (e) h_{PM}. (f) w_{st}.

As to d_{rotor}, the initial value is set to 100 mm, with a varied range of 80 mm $\sim$ 120 mm. For d_{stator}, the initial value is set to 345 mm while the variation range is from 335 mm to 395 mm. For l_{gap}, 1.1 mm is taken as the initial value, and the range is from 0.9 mm to 1.2 mm. Finally, for w_{st}, the initial value is set to 5° with a variation range of 4.5° $\sim$ 6.5°. The initial values and ranges are tabulated in Table 8.

Table 8. Initial values and ranges of the optimization variables.

Variable	Initial Value	Variance Range
d_{rotor}/mm	100	$80 \sim 120$
d_{stator}/mm	345	$335 \sim 395$
l_{gap}/mm	1.1	$0.9 \sim 1.2$
w_{st}/deg	5°	$4.5° \sim 6.5°$

3.3. Globalized Optimization Based on GA Method

In this section, GA is combined with FEM simulations for the optimization of the Taguchi-per-optimized motor. In addition, the optimization variables and their ranges are also selected based on Taguchi analyses.

In the GA-based global optimization processes, the averaged output torque is taken as the objective function. The optimization converges when the fitness function meets the following conditions:

$$|T^*(G+1) - T^*(G)| < 0.0005\,|T^*(G)| \tag{4}$$

where $T^*(G)$ (in kN·m) means the fitness function value of the best individual in the Gth generation. In this paper, a very critical criterion ($5‰$) is taken as the GA-based optimization can converge fluently with the Taguchi-preconditioned initial values and variables, as shown in Fig. 7.

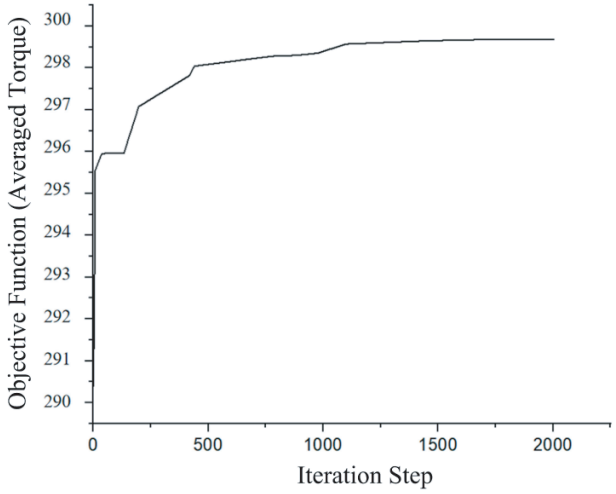

Figure 7. Convergence curve.

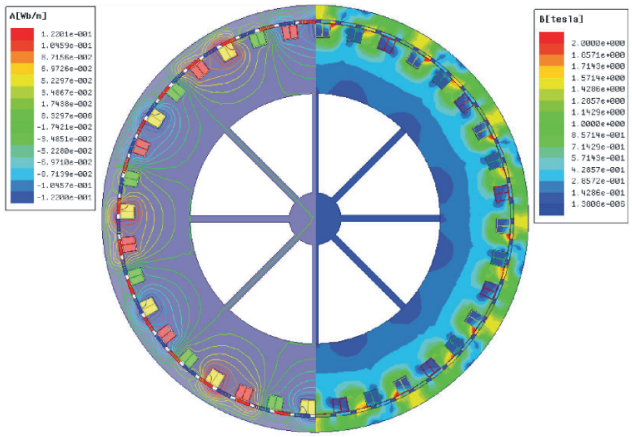

Figure 8. Electromagnetic performances of the PMVM with optimized structural parameters.

Figure 8 shows the flux lines and flux density distributions of the PMVM with optimized structural configuration. When the motor is working under full-load operations, the output torque curve and back EMF curves versus time are shown in Fig. 9 and Fig. 10, respectively. As obtained from the simulation results, T_{ave} is 296.94 kN·m with T_{rip} at 3.40 kN·m, and U_{ave} is 13.60 kV. Table 9 tabulates the optimized structural parameters and related working characteristics. As can be found from the table, the PMVM can output larger torque after the TPGA processes.

3.4. Validation

In order to validate the FEA techniques used in this paper, the methodologies are used to calculate the working performances of a 2.1-kW PMSM prototype with an amorphous alloy (AA) stator core [24]. Fig. 11 illustrates the test bench of the machine. The electromagnetic field of the machine is shown

Table 9. Comparison between initial and optimized values.

Variable	Initial	Taguchi-preliminarily optimized	GA optimized
d_{rotor}/mm	100	100	92.5
d_{stator}/mm	345	345	348.1
l_{gap}/mm	1	1.1	0.95
h_{st}/mm	85	90	90
h_{pm}/mm	20	18.6	18.6
w_{st}/deg	5.5°	5°	5.5°
T_{ave}/kN·m	283.93	291.34	296.94

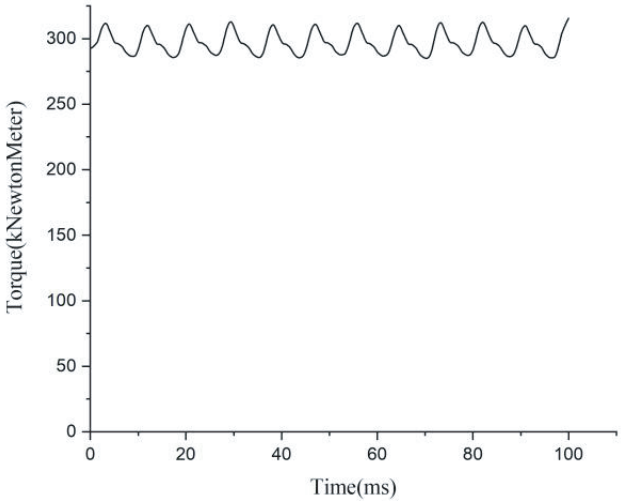

Figure 9. The output torque versus time (GA optimized).

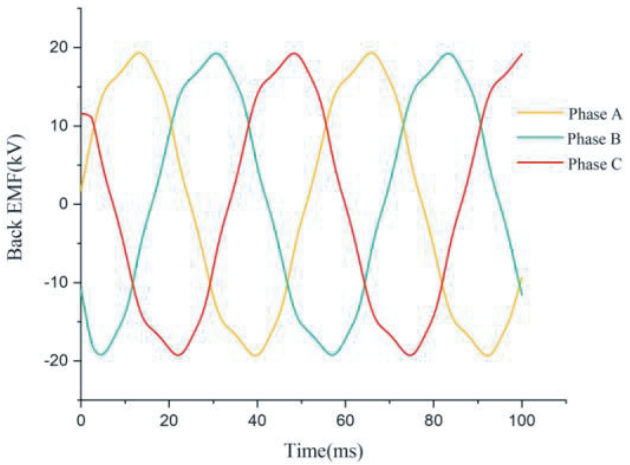

Figure 10. The back-EMF versus time (GA optimized).

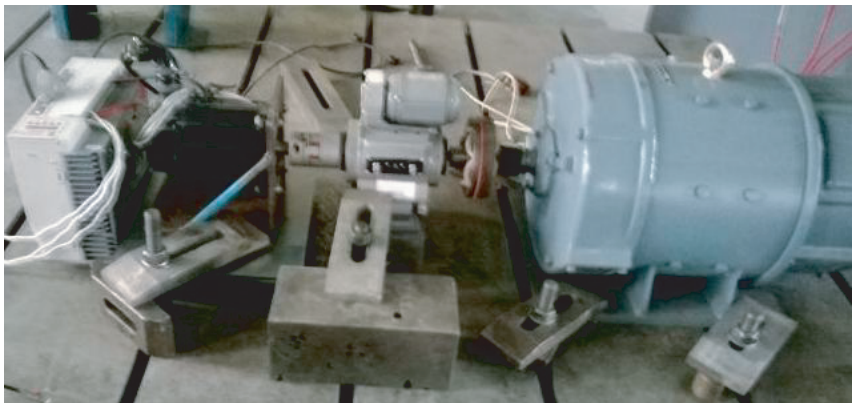

Figure 11. Experimental setup.

in Fig. 12, and the calculated and tested no-load back EMF values are compared in Table 10. As the calculated results can fit in well with the tested ones, the numerical simulation methods used in this paper are indirectly validated.

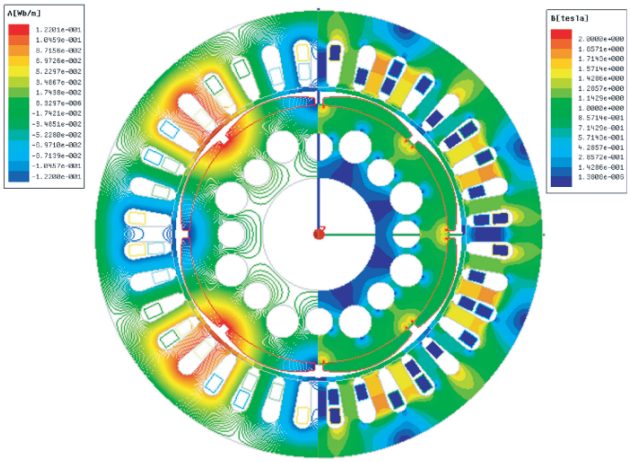

Figure 12. Flux lines and flux density distributions of the 2.1-kW PMSM.

Table 10. Comparison between calculated and tested no-load back EMF.

Value	Calculated	Tested	Error
Back EMF (in rms)	233 V	226 V	3.10%

4. CONCLUSION

This paper proposes a TPGA strategy coupling Taguchi method and GA for the optimal design of a 630-kW PMVM. The working performances of the machine with initial structural parameters are firstly analyzed through FEA. The calculation results show that the PMVM can provide a large torque density even with the initial parameters. Taguchi method is employed to find the influence factors of six typical optimization variables (rotor yoke depth, stator yoke depth, air-gap length, stator tooth height, PM height, and stator tooth width) on the output torque. In addition, a preliminary optimization result is also obtained through Taguchi analyses. GA is then utilized to realize the global optimization of the PMVM. During the GA-based optimization processes, four variables (rotor yoke depth, stator yoke depth, air gap length, and stator teeth width) with relatively large influence factors are selected as the optimization variables, and the Taguchi-preliminarily optimized structural parameters are taken as the initial values. As the optimization variable number is limited to a fine initial value, the calculation burden caused by the FEA in the GA-based global optimization can be effectively reduced. After the TPGA optimization process, the output torque of the PMVM is improved by 13.01 kN·m compared with that of the machine with initial parameters, which proves the effectiveness of the proposed methodology.

REFERENCES

1. Jian, L. N., W. S. Gong, G. Q. Xu, J. N. Liang, and W. X. Zhao, "Integrated magnetic-geared machine with sandwiched armature stator for low-speed large-torque applications," *IEEE Trans. Magn.*, Vol. 48, No. 11, 4184–4187, Nov. 2012.
2. Liu, C. T., K. Y. Hung, and C. C. Hwang, "Developments of an efficient analytical scheme for optimal composition designs of tubular linear magnetic-geared machines," *IEEE Trans. Magn.*, Vol. 52, No. 7, Art. No. 8202404, Jul. 2016.
3. Fang, Y. N., X. H. Liang, and M. J. Zuo, "Effect of sliding friction on transient characteristics of a gear transmission under random loading," *Proc. 2017 IEEE International Conference on Systems, Man, and Cybernetics (SMC)*, 2551–2555, Banff, AB, Canada, Nov. 2017.

4. Chen, S. Q., J. Y. Zhao, B. W. Li, Z. Xu, and Y. Q. Feng, "Nonlinear dynamic model and governing equations of low speed and high load planetary gear train with respect to friction," *Proc. 2011 International Conference on Consumer Electronics, Communications and Networks (CECNet)*, 3274–3278, Xianning, China, Apr. 2011.
5. Atallah, K. and D. Howe, "A novel high-performance magnetic gear," *IEEE Trans. Magn.*, Vol. 37, No. 4, 2844–2846, Jul. 2001.
6. Cooke, G., R. S. Dragan, R. Barrett, D. J. Powell, S. Graham, and K. Atallah, "Magnetically geared propulsion motor for subsea remote operated vehicle," *IEEE Trans. Magn.*, Vol. 58, No. 2, Art. No. 8201005, Feb. 2022.
7. Fu, W. N. and S. L. Ho, "A quantitative comparative analysis of a novel flux-modulated permanent-magnet motor for low-speed drive," *IEEE Trans. Magn.*, Vol. 46, No. 1, 127–134, Jan. 2010.
8. Li, J. G. and K. T. Chau, "Performance and cost comparison of permanent-magnet vernier machines," *IEEE Trans. Magn.*, Vol. 22, No. 3, Art. No. 5202304, Jun. 2012.
9. Toba, A. and T. A. Lipo, "Generic torque-maximizing design methodology of surface permanent-magnet vernier machine," *IEEE Trans. Ind. Appl.*, Vol. 36, No. 6, 1539–1546, Nov./Dec. 2000.
10. Zhao, X., S. X. Niu, and W. N. Fu, "Torque component quantification and design guideline for dual permanent magnet vernier machine," *IEEE Trans. Magn.*, Vol. 55, No. 6, Art. No. 8101905, Jun. 2019.
11. Ma, Y., Y. Xiao, J. Wang, and L. Zhou, "Multicriteria optimal Latin hypercube design-based surrogate-assisted design optimization fora permanent-magnet vernier machine," *IEEE Trans. Magn.*, Vol. 58, No. 2, Art. No. 8101205, Feb. 2022.
12. Feng, G. D., C. Y. Lai, M. Kelly, and N. C. Kar, "Dual three-phase PMSM torque modeling and maximum torque per peak current control through optimized harmonic current injection," *IEEE Trans. Ind. Electron.*, Vol. 66, No. 5, 3356–3368, May 2019.
13. Lai, C. Y., G. D. Feng, K. L. V. Iyer, K. Mukherjee, and N. C. Kar, "Genetic algorithm-based current optimization for torque ripple reduction of interior PMSMs," *IEEE Trans. Ind. Appl.*, Vol. 53, No. 5, 4493–4503, Sept./Oct. 2017.
14. Lin, Q. F., S. X. Niu, and W. N. Fu, "Design and optimization of a dual-permanent-magnet vernier machine with a novel optimization model," *IEEE Trans. Magn.*, Vol. 56, No. 3, Art. No. 7512705, Mar. 2020.
15. Wang, Q. L., F. Zhao, and K. Yang, "Analysis and optimization of the axial electromagnetic forcefor an axial-flux permanent magnet vernier machine," *IEEE Trans. Magn.*, Vol. 57, No. 2, Art. No. 8100605, Feb. 2021.
16. Sorgdrager, A. J., R. J. Wang, and A. J. Grobler, "Multiobjective design of a line-start PM motor using the Taguchi method," *IEEE Trans. Ind. Appl.*, Vol. 54, No. 5, 4167–4176, Sept./Oct. 2018.
17. Giurgea, S., D. Fodorean, G. Cirrincione, A. Miraoui, and M. Cirrincione, "Multimodel optimization based on the response surface of the reduced FEM simulation model with application to a PMSM," *IEEE Trans. Magn.*, Vol. 44, No. 9, 2153–2157, Sept. 2008.
18. Shin, P. S., S. H. Woo, Y. L. Zhang, and C. S. Koh, "An application of Latin hypercube sampling strategy for cogging torque reduction of large-scale permanent magnet motor," *IEEE Trans. Magn.*, Vol. 44, No. 11, 4421–4424, Nov. 2008.
19. Sun, X., Z. Shi, and J. Zhu, "Multiobjective design optimization of an IPMSM for EVs based on fuzzy method and sequential Taguchi method," *IEEE Trans. Ind. Electron.*, Vol. 68, No. 11, 10592–10600, Nov. 2021.
20. Zhu, G. J., L. N. Li, Y. H. Mei, T. Liu, and M. Xue, "Design and analysis of a self-circulated oil cooling system enclosed in hollow shafts for axial-flux PMSMs," *IEEE Trans. Veh. Technol.*, Vol. 71, No. 5, 4879–4888, May 2022.
21. Khan, M. A., I. Husain, M. R. Islam, and J. T. Klass, "Design of experiments to address manufacturing tolerances and process variations influencing cogging torque and back EMF in the mass production of the permanent-magnet synchronous motors," *IEEE Trans. Ind. Appl.*, Vol. 50, No. 1, 346–355, Jan./Feb. 2014.

22. Xia, C. L., L. Y. Guo, Z. Zhang, T. N. Shi, and H. M. Wang, "Optimal designing of permanent magnet cavity to reduce iron loss of interior permanent magnet machine," *IEEE Trans. Magn.*, Vol. 51, No. 12, Art. No. 8115409, Dec. 2015.
23. Shi, Z., X. Sun, Y. Cai, and Z. Yang, "Robust design optimization of a five-phase PM hub motor for fault-tolerant operation based on Taguchi method," *IEEE Trans. Energy Convers.*, Vol. 35, No. 4, 2036–2044, Dec. 2020.
24. Zhu, G. J., Y. H. Zhu, W. M. Tong, X. Y. Han, and J. G. Zhu, "Thermal analysis techniques of finite formulation method and the application on permanent magnet machines," *Proceedings of the CSEE*, Vol. 37, No. S1, 152–161, Sept. 2017.